Electrical Images of the Forrestania Greenstone Belt

Shane Evans – Moombarriga Geoscience

Bill Amann – Newexco Service

Mike Dentith – Centre for Exploration Targeting, University of Western Australia

Introduction

Magnetotelluric (MT) and audio-magnetotelluric (AMT) data were collected across the Forrestania Greenstone Belt (FGB) of Western Australia. This survey complements a regional and ongoing MT survey between Hyden and Norseman designed to investigate the lithospheric structure of the southern Yilgarn Craton. Results from this regional survey identify a crustal conductor spatially coincident with the FGB and prompts the acquisition of high-resolution data to resolve this feature in greater detail.

The FGB, which corresponds to the southern extension of the Southern Cross greenstone belt, is located ca. 350 kms east of Perth (Figure 1). The FGB comprises a lower sequence of tholeiite-komatiite-banded iron formation, overlain by an upper sequence of felsic metasediments (Collins and McCuaig, 2010). Nickel sulphide deposits occur over a 90km strike length of the greenstone belt within three of the six ultramafic belts of predominantly komatiite rock-types (Figure 2). These ultramafic belts have a high magnetic response and are well defined in regional magnetic maps.

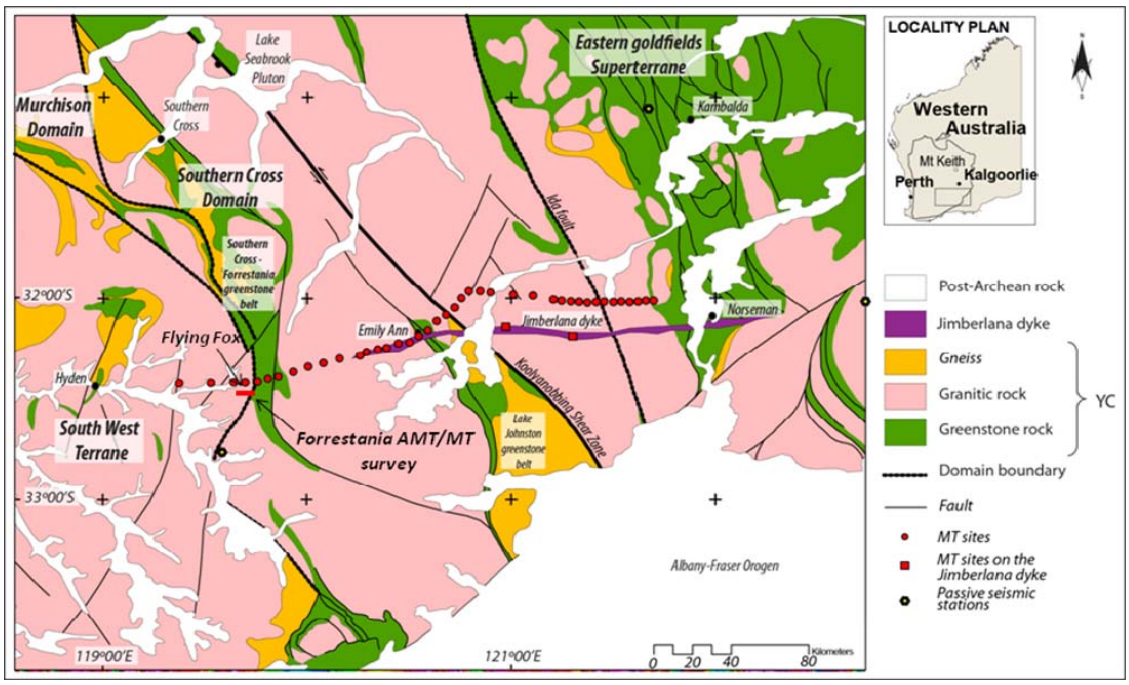

Figure 1: Regional geology map of the southern Yilgarn Craton.

The recently discovered Flying Fox and Spotted Quoll nickel sulphide deposits are hosted within the Western Ultramafic belt (Perring et al, 1996). This belt dips from 40^{o} to 80^{o} east and comprises a footwall sequence dominated by psammitic to pelitic schists. The footwall is in turn overlain by a differentiated suite of komatiite rock-types, basalt and banded iron formation. This differentiated suite is sulphidic and associated to a continuous conductive horizon well-known from down-hole and surface transient EM surveys.

The objective of the AMT/MT survey is to map this conductive horizon at depth and to determine the structural relationships between the Western Ultramafic belt and the others. By assuming the horizon is as conductive and extensive down dip as it is along strike one could postulate on the entire belts architecture.

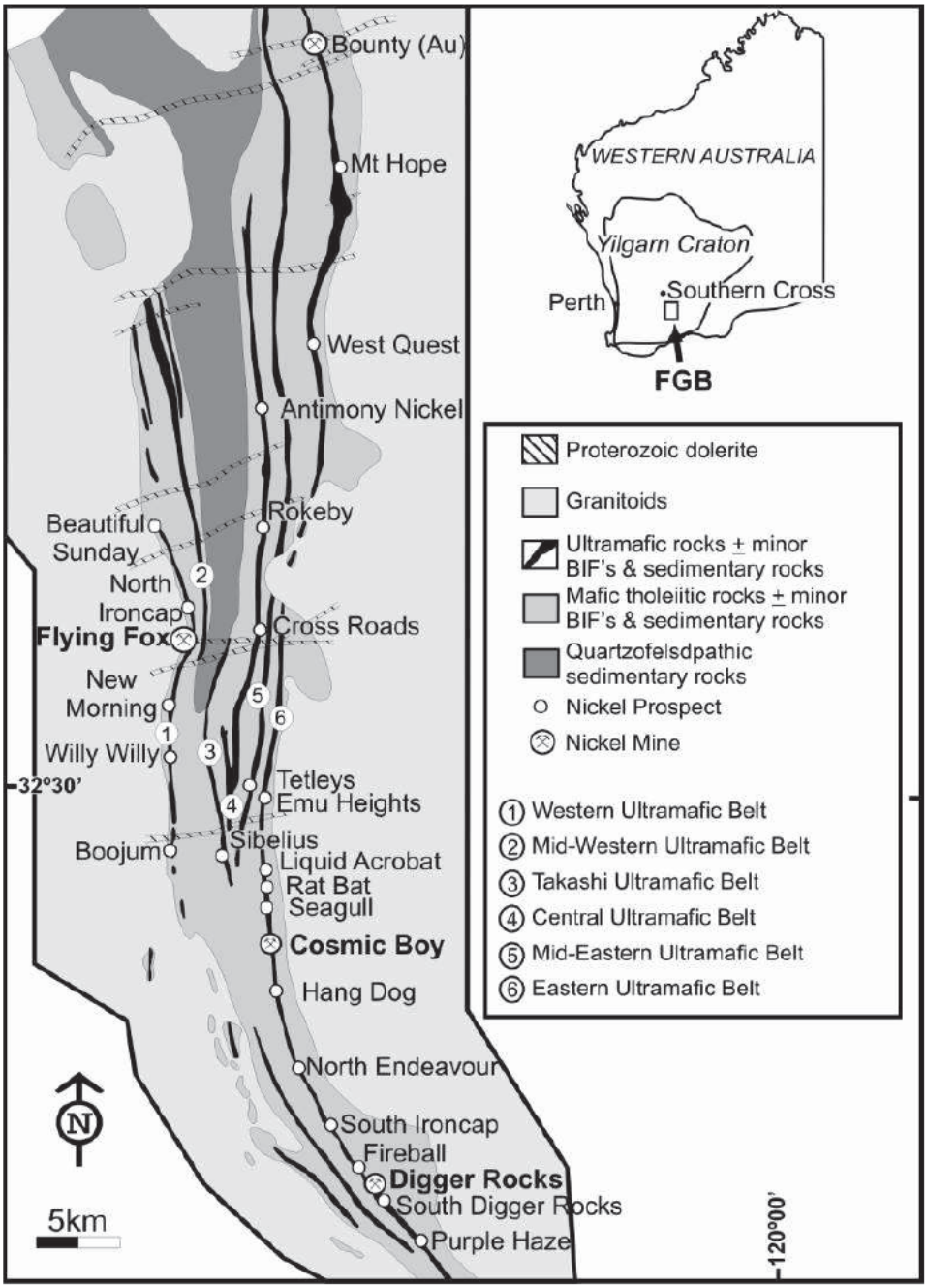

Figure 2: Simplified geological map (from Collins and McCuaig 2010).

Magnetotellurics

The MT method measures the time-variations in the natural electromagnetic (EM) field at the surface of the Earth. Low-frequency variations (1 – 0.0001 Hz) in the EM field are primarily caused by solar wind interacting with the terrestrial magnetic field, whereas high-frequency variations (>1 Hz) are caused by distance lightning storms. The EM field comprises a magnetic field $(\overline{H})$ and an associated electric field $(\overline{E})$. By Faraday's Law of induction, this time-varying magnetic field induces an electric field within the Earth, and, in turn, by Ohm's Law the electric field generates an electric current. The scaled magnitude ratio of the electric and magnetic fields, as well as the phase differences between the electric and magnetic fields, at a number of sites are utilized to determine the sizes and locations of zones of enhanced conductivity. The MT impedance tensor (Z) describes the relationship between orthogonal components of the horizontal electromagnetic field (Ex, Ey, Hx and Hy) at a given frequency such that

$$\begin{pmatrix} E_x \\ E_y \end{pmatrix} = \begin{pmatrix} Z_{xx} & Z_{xy} \\ Z_{yx} & Z_{yy} \end{pmatrix} \begin{pmatrix} H_x \\ H_y \end{pmatrix}$$

In the 1-D case $Z_{xy} = -Z_{yx}$ with Z_{yy} and $Z_{xx} = 0$. In a 2-D Earth, if either $\overline{E}$ or $\overline{H}$ is along geoelectric strike, then Z_{yy} and Z_{xx} will = 0 and $Z_{xy} \neq -Z_{yx}$. If $\overline{E}$ or $\overline{H}$ are not along the strike then H_x will generate $\overline{E}$ in both the *x* and *y* directions, likewise H_y will generate $\overline{E}$ in both the *x* and *y* directions (i.e. Z_{yy} and Z_{xx} are nonzero).

Apparent resistivity (ρ) and the phase lead (φ) of the electric field over the magnetic field can also be calculated through the relationships

$$\rho_{xy} = \frac{1}{\mu\omega}\left|\frac{E_x}{H_y}\right|^2,$$

$$\rho_{xy} = \frac{1}{\mu\omega}\left|Z_{xy}\right|^2,$$

$$\phi_{xy} = \arctan\left|\frac{E_x}{H_y}\right|,$$

where μ is the magnetic permeability of free air and ω is the angular frequency.

As an EM wave propagates through the Earth, its amplitude will decay at a rate dependent on the conductivity of the medium and the rate of time variation of the wave, such that information about the near-surface is obtained from high-frequency variations and deep structure obtained from low-frequency variations. In a half-space of uniform resistivity, the depth at which an EM wave decays to 1/e of its original value is known as the "skin depth" (δ) and is an approximate measure for the depth of penetration.

$$\delta = \sqrt{\frac{2}{\mu\sigma\omega}},$$

where σ is the conductivity (1/resistivity(ρ)).

The electrical resistivity (ρ) of rocks can vary by over eight orders of magnitude (>100,000–<0.001 Ωm). Figure 3, modified from Haak & Hutton (1986), gives an overview of the typical ranges of resistivity and conductivity for various types of rocks. Typically, competent, unfractured, crystalline rocks within the continental crust have a high resistivity (~100,000 Ωm), but values less than this are often observed. Regions of low resistivity can be attributed to the presence of interconnected conductive material that is, typically, a minor component of the whole rock. Electrical conduction within the

Earth can be attributed to either ionic conduction (movement of charged particles) or electronic conduction (movement of electrons). Ionic conduction may be due to the presence of partial melts along grain boundaries or saline water filling pore space or intruding along fracture zones (Jones, 1992). Electronic conduction generally occurs when interconnected graphite, sulphide or iron ores occur within a rock.

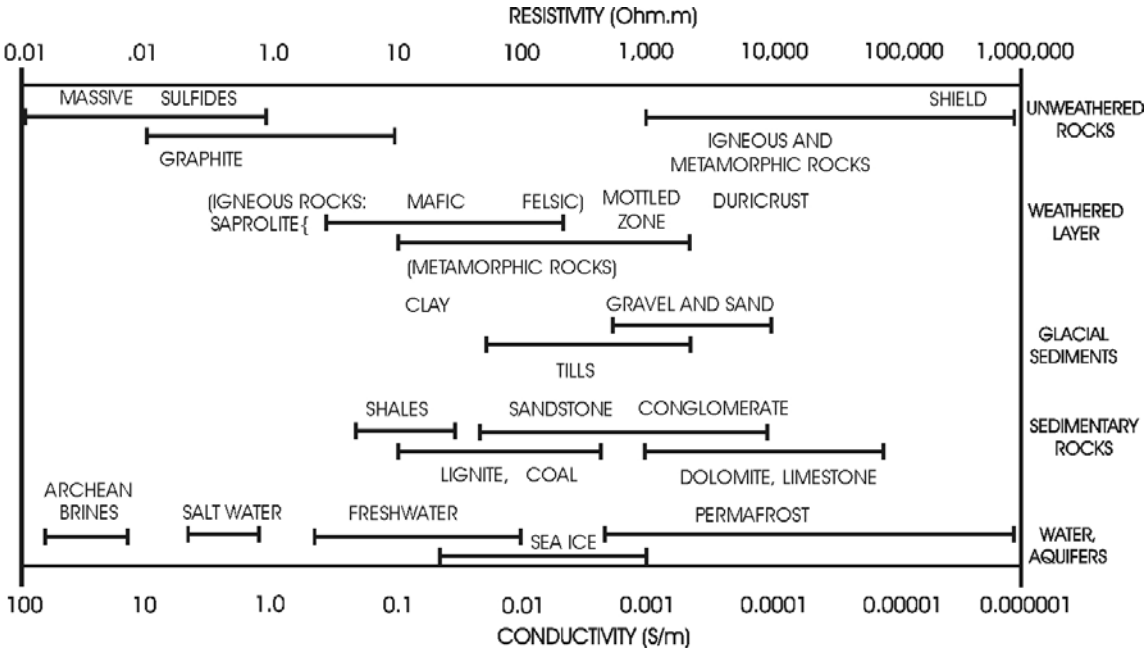

Figure 3: Conductivity and resistivity ranges for various rock types (modified from Haak and Hutton 1986).

Regional MT Data

A magnetotelluric survey, comprising 40 stations, has been completed in the southern Yilgarn Craton (Figure 1). The preferred resistivity cross section through the crust shows the local lithosphere comprises three distinct units separated by steep boundaries. The central unit (Unit 2), interpreted as equivalent to the Southern Cross Domain has a resistive crust overlying a more conductive mantle. The two units on either side (Unit 1

(western) and Unit 3 (eastern)) comprise a conductive lower crust overlying a resistive mantle. Dipping narrow zones of increased conductivity in the crustal part of the model correlate with known surface structures (A-H). Feature A is coincident with the location of the FGB and is the focus of this paper. The eastern margin of the Southern Cross Domain as inferred from deep crustal and mantle resistivity occurs about 50 km to the west of the Ida Fault, the margin of the domain at the surface. The three fold subdivision of the local lithosphere is consistent with the geologically and geochemically defined terranes and domains in this part of the Yilgarn. Features I and J are conductive regions on the lower crust or top of the upper mantle that are characteristic of Unit 3 and Unit 2

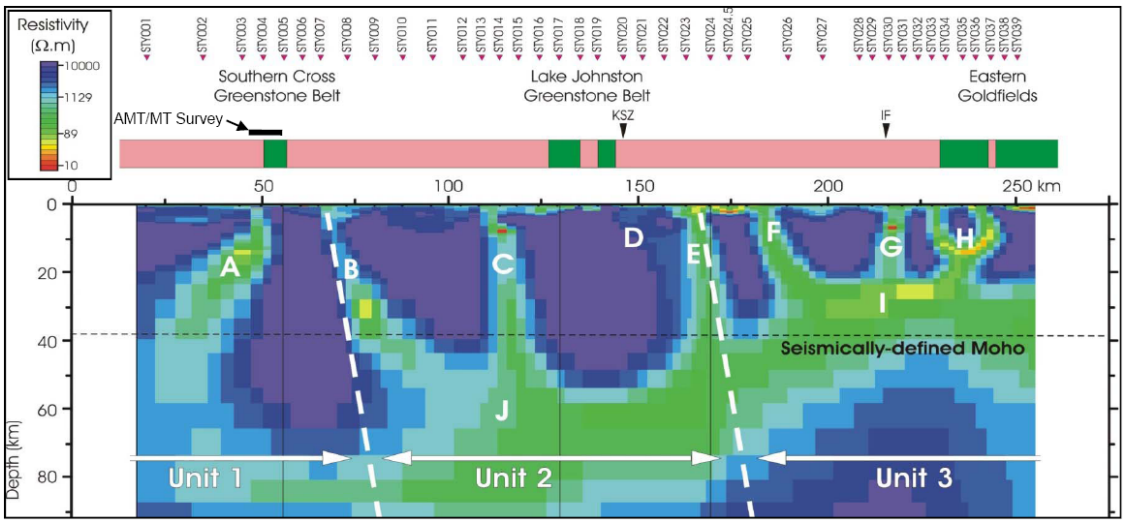

Figure 4: 2D resistivity model from regional MT survey (modified from Dentith et al, 2011).

AMT/MT Acquisition and Processing

During December 2010, AMT and MT data were collected at 31 sites along a 10km-long profile with a site spacing of 250 metres. Three components of the magnetic field (Hx,

Hy and Hz) and 2 components of the electric (Ex and Ey) field were recorded at all sites except at sites where the Hz component was omitted because of difficult digging conditions (see Figure 5 for a typical site setup). AMT data were acquired at all sites and MT data were collected at 11 sites (approximately every third site). Phoenix-made MTU-5A data recorders were used with MTC-50 induction coils for MT recordings and MTC-30 induction coils for AMT recordings. MT data were recorded for at least 12 hours and AMT data for approximately 1 hour.

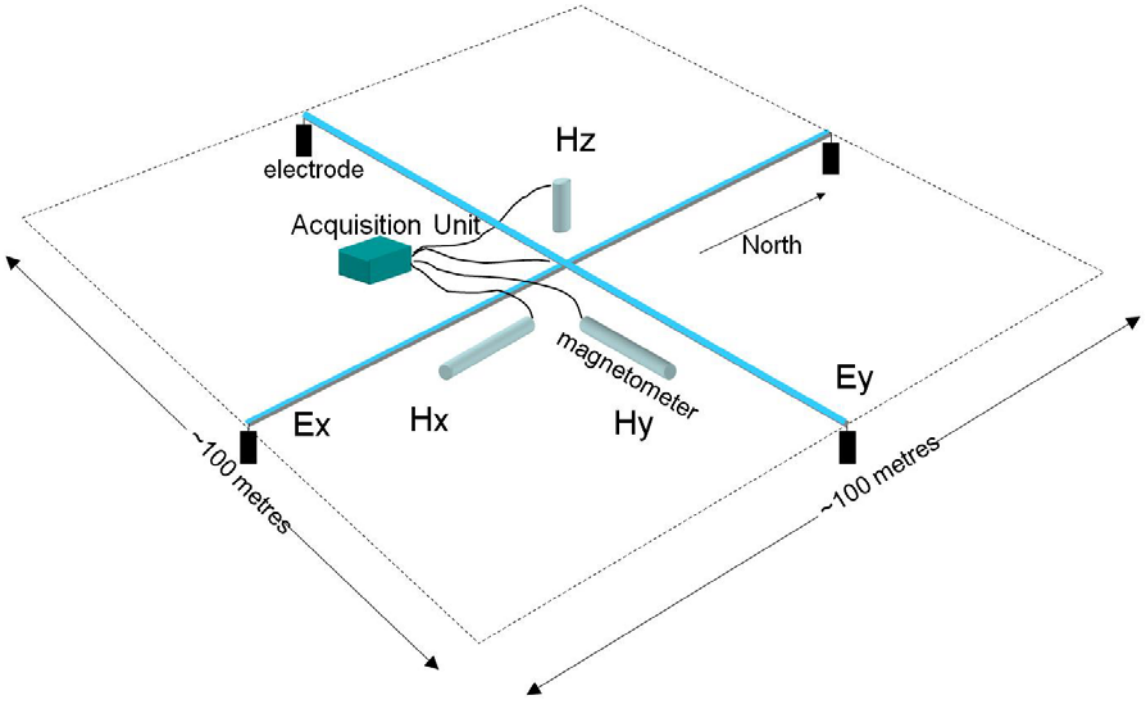

Figure 5: Typical MT site setup.

The time-series data were processed using robust remote-reference algorithms supplied by Phoenix Limited and based on the coherence-sorted cascade decimation method of Jones and Jödicke (1984). Remote reference processing (Gamble et al., 1979) used a simultaneously recording station within the profile. Processed data resulted in apparent

resistivity and phase curves in the band 10,000-5 hz for the AMT recording and 200-0.01hz for the MT recording.

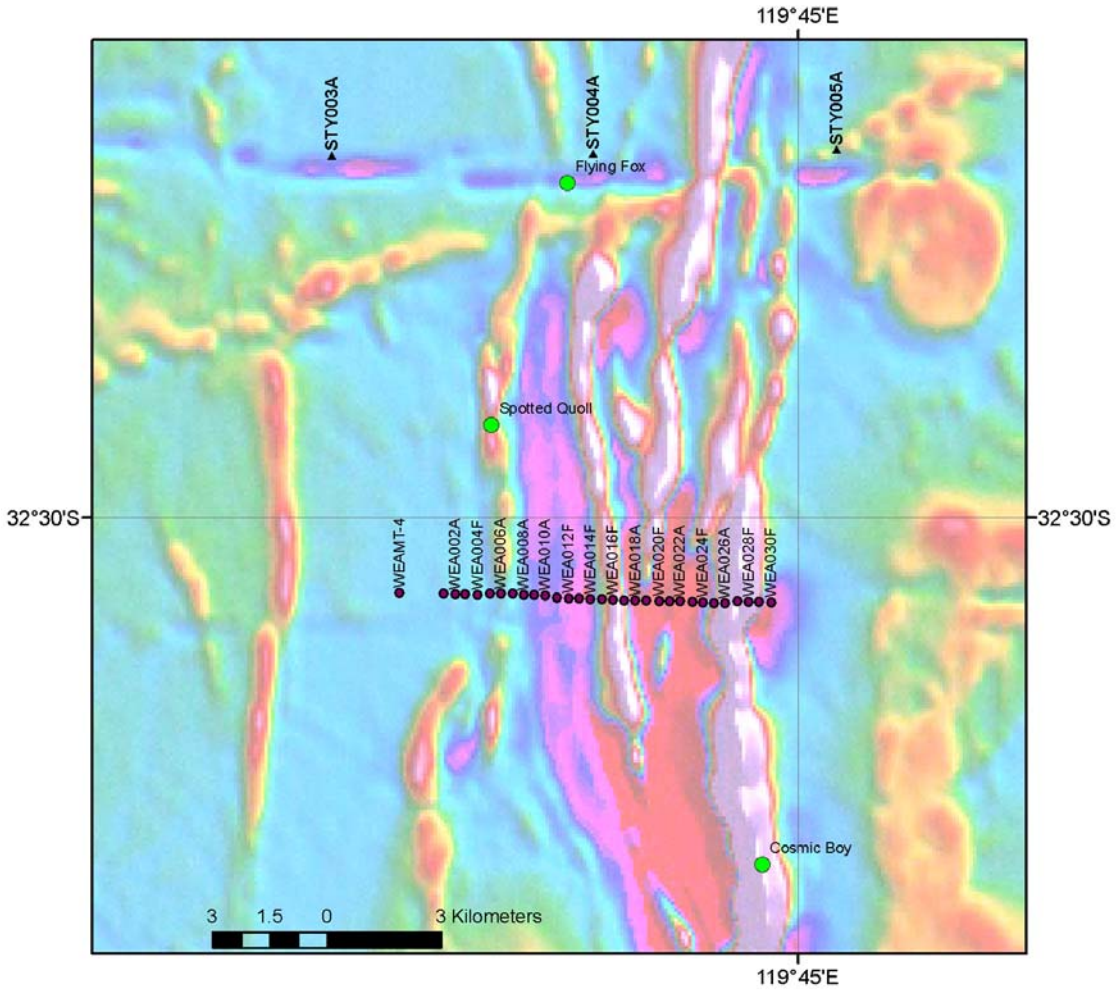

Figure 6: AMT/MT site locations (red dots), regional MT site locations (black triangles) and nickel mines (green circles) with regional magnetic as the background.

Modeling

These data were modeled using the 2D non-linear conjugate gradient inversion algorithm of Rodi and Mackie (2001) as implemented in the Winglink™ software package (Geosystem SRL, 2008). This inverse modelling method minimizes an objective function

consisting of the data misfit and a measure of model roughness, with the user-specified trade-off parameter, τ, defining the balance between these terms. Both TE and TM modes and the modelled over the frequency range 200-0.01hz. These data were inverted assuming a north-south strike direction which is the known geological strike direction. The resulting resistivity model can be seen in Figure 7.

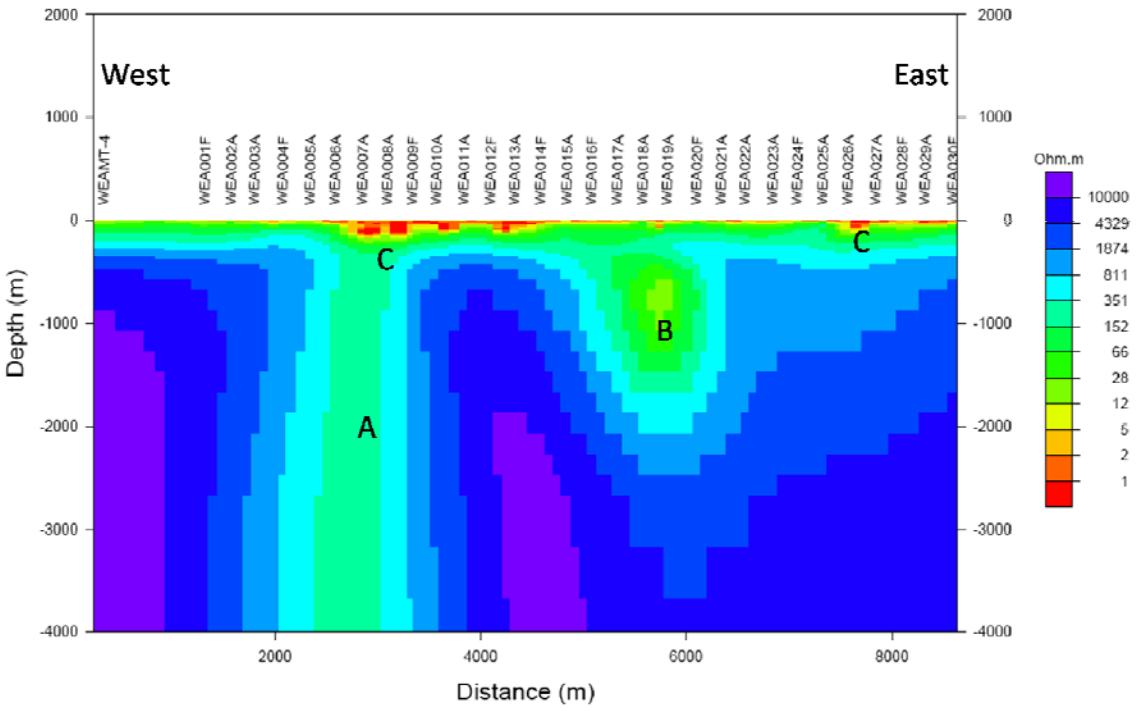

Figure 7: 2D Resistivity model. Features A, B and C are discussed in the text.

Interpretation

Feature A from Figure 7 is spatially coincident with the Western Ultramafic belt that is known to be conductive. The model shows Feature A to be steeply dipping to the west. It should be noted that the dip of sub-vertical conductors is not well resolved using MT so a

conductor dipping steeply to the east may also fit the data. Feature B appears to be a response to the southern end of the Central Ultramafic belt (Figure 2). During the modeling process it could be seen that feature B was not robust and a conductor could be located at various locations between sites 17 and 20 at depths between 500-1500m and still fit the data to an acceptable degree. This may due to the local 3D nature of the geology in the area. It can be seen in Figure 6 that the Central Ultramafic belt which is defined by the highly magnetic linear feature north of site 19 does not appear to cross the survey line. The MT sites in this area may be detecting features that are not directly beneath the profile and may make the 2D assumption that is required for inversion invalid to some degree and therefore difficult to generate a robust 2D model. Features C can be related to clays that have weathered from the ultramafic belts or BIF at the near surface.

Conclusion

The Western Belt contains a highly conductive horizon as expected. This horizon does not dip to the east at 45 degrees under the central belts as could be expected from the deep drilling results at Spotted Quoll. The conductor appears to be truncated to the east and continues steeply to at least 5 kilometres. This could be explained by a fault repetition of the horizon displaced below the present position or an overturning of the sequence to a westerly dip. Interpretation of the inversion results suggests that the conductive horizon, if present, does not extend to depth on the other ultramfic belts. Only the Central Belt has some evident of enhanced conductivity at depth but is not well resolved in this model. One could then assume that the other ultramafic belts maybe

lacking in the sulfides that enhance the electrical conductivity of the belt and in turn may be less economical prospective.

The electrical model of the FGB (Figure 7) appears to agree well with the model produced from the regional MT survey (Figure 4). The regional model suggests that the conductor extends through to the Moho. One could reasonable assume that the Western Belt does not extent to the base of the crust but could postulate that the Western Belt and most likely the entire FGB is intimately linked to a crustal fracture or boundary.

References

Collins, J.E., McCuaig, C.C. 2010, The Flying Fox Ni-Cu-PGE komatiite-hosted deposit, Forrestania Greenstone Belt (Chapter 7) in Record 2010/26: Controls on giant mineral systems in the Yilgarn Craton – A field guide, Geological Survey of Western Australia , Perth.

Dentith, M, Evans, S, Thiel, S, Luis Gallardo, L and Joly, A, 2011, A magnetotelluric traverse across the southern Yilgarn Craton. GSWA Report submitted.

Gamble, T.D., Goubau, W.M., and Clark, J., 1979, Magnetotellurics with a Remote Reference: Geophysics, 44: 53.

Haak, V., and Hutton, V.R.S., 1986. Electrical resistivity in continental lower crust. The Nature of the Lower Continental Crust, eds., J.B. Dawson, D.A. Carswell, J. Hall and K.H. Wedepohl. Geol. Soc. London, Sp. Publ. 24: 35 49.

Jones, A.G., 1992. Electrical conductivity of the continental lower crust. In: Continental Lower Crust, eds., D.M. Fountain, R.J. Arculus and R.W. Kay. Elsevier, Amsterdam, Chapter 3: 81 143.

Jones, A.G, and Jödicke, H 1984, Magnetotelluric transfer function estimation improvement by a coherence based rejection technique, in Abstract Volume of the 54th Society of Exploration Geophysics Annual General Meeting, Atlanta, Georgia, 51–55.

GEOSYSTEM SRL 2008. WinGLink® User's Guide, GEOSYSTEM SRL, Milan, Italy.

Perring C.S, Barnes S.J, Hill R.E.T., (1996) Geochemistry of Archaean komatiites from the Forrestania Greenstone Belt, Western Australia: evidence for supracrustal contamination. Lithos 37:181-197

Rodi, W, and Mackie, R.L, 2001. Nonlinear conjugate gradients algorithm for 2-D magnetotelluric inversion: Geophysics, v. 66, 174–187.